Thermochimica Acta, 204 (1992) 99–110
Elsevier Science Publishers B.V., Amsterdam

Thermobarometric and differential scanning calorimetric study of the polymorphism of some even and odd paraffins (C_{26}, C_{27}, C_{40}, C_{60}) [1]

D. Lourdin [a], A.H. Roux [a], J.-P.E. Grolier [a] and J.-M. Buisine [b]

[a] *Laboratoire de Thermodynamique et Cinétique Chimique (URA CNRS 434), Université Blaise Pascal, 63177 Aubière Cedex (France)*
[b] *Laboratoire de Dynamique des Cristaux Moléculaires (URA CNRS, 801) Université des Sciences et Techniques de Lille Flandre-Artois, 59655 Villeneuve d'Ascq Cedex (France)*

(Received 11 September 1991; in final form 17 December 1991)

Abstract

Thermal and thermobarometric analysis of three *n*-paraffins having an even number of carbon atoms (C_{26}, C_{40} and C_{60}) and of one paraffin having an odd number (C_{27}) are reported. The two techniques used yield consistent results in agreement with high-pressure literature data. The thermobarometric technique allows one to detect low-enthalpy or weak transitions, especially in the case of the short paraffins exhibiting more complex phase diagrams. It appears that the stability domain with respect to pressure and temperature of the rotative phase, which is stable in the fusion vicinity for paraffins, decreases when the pressure and/or the chain length increases.

INTRODUCTION

Long chain *n*-alkanes or paraffins (C_nH_{2n+2}) are of great importance in the petroleum industry because of their presence in crude oil and gas oil. These molecules are also important as model molecules of some simple polymers [2]. The knowledge of their physical properties as functions of temperature and pressure and, more generally, the knowledge of their P–T phase diagrams is then essential. Several studies have been devoted to the establishment of the (P–T) phase diagrams of pure paraffins, using a wide range of techniques. Very often differential thermal analysis has been used to measure the energetic modifications associated with the observed phase transitions [3–5].

Correspondence to: D. Lourdin, Laboratoire de Thermodynamique et Cinétique Chimique (URA CNRS 434), Université Blaise Pascal, 63177 Aubière Cedex, France.

[1] This paper was presented during the 22nd annual meeting of the French Association of Calorimetry and Thermal Analysis (AFCAT) at Paris-XI–Châtenay-Malabry (27–29 May 1991).

TABLE 1

Stated purities and origins of pure components. Temperatures of fusion T_f and of transition T_{tr} in °C as measured by differential thermal analysis (DSC) or by thermobarometric analysis (metabolemeter); values in parentheses are from the literature

	DSC			Metabolemeter	Purity	Manufacturer
$C_{60}H_{122}$						
T_f	100.0	(99.6) [2]		100.5	> 98%	Fluka
$C_{40}H_{82}$						
T_f	80.0	(81.4) [2]	(81.6) [3]	80.6	99%	Sigma
T_{tr}	72.2			73.5		
$C_{26}H_{54}$						
T_f	55.0	(56.5) [5]		57.3	99%	Fluka
T_{tr}	51.2	(51.1) [5]		50.6		
$C_{27}H_{56}$						
T_f	58.5	(59.5) [3]	(60.6) [4]	58.8	99%	Fluka
T_{tr_1}	52.2	(53.5) [3]	(53.9) [4]	53.4		
T_{tr_2}	45.4	(46.3) [3]	(44.8) [4]	45.3		

It is known that paraffins may show very different phase diagrams depending on their number of methylene groups and whether this number is odd or even. However, although the temperature effects on these phase diagrams have been quite well investigated, the effect of pressure has seldom been taken into consideration.

In this work we have selected four paraffins, three with even numbers of carbon atoms (C_{26}, C_{40}, C_{60}) and one with an odd number (C_{27}), in order to check the possibilities of using a new thermobarometric technique. To detect the structural transitions at atmospheric pressure we used a differential temperature scanning calorimeter. The pressure effect upon the structural changes has been evaluated using a thermobarometric analyser recently developed by Buisine et al. [1]. This technique allows one to obtain directly the boundary $P = f(T)$ curves between the existing phases.

EXPERIMENTAL

Chemicals

The compounds studied were hexacosane ($C_{26}H_{54}$), heptacosane ($C_{27}H_{56}$), tetracontane ($C_{40}H_{82}$) and hexacontane ($C_{60}H_{122}$). Their origins together with their respective stated purities are indicated in Table 1. They were used without further purification. Their temperatures of fusion T_f and of solid–solid transition T_{tr} are given in Table 1, together with literature values for comparison.

Experimental

Two instruments were used: a differential temperature scanning calorimeter and a thermobarometric analyser.

The temperatures corresponding to a phase change at atmospheric pressure were determined with a DSC 111 Setaram calorimeter. This calorimeter is based on the well-known Calvet principle using a differential detection of the thermal flux between the measuring and the reference cells and the thermoregulated block. The temperature scanning of the block is programmed by means of a computer, which also collects and stores the data of the measured flux. Each experiment was carried out under argon at the same normalized temperature scanning rate (1°C min^{-1}) on a sample of about 5 mg. In these conditions, the reproducibility

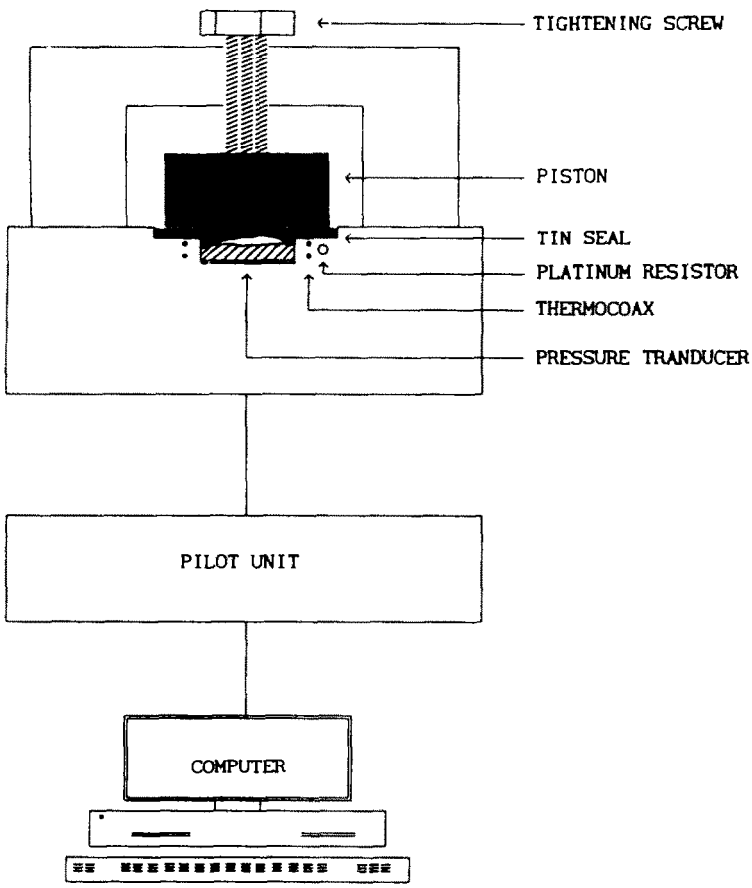

Fig. 1. Scheme of the thermobarometric technique using an MTM Leader Metabolemeter. The free volume corresponds to the space between the product (striped) and the seal (dark).

of the characteristic temperatures was about ±0.1°C, as obtained from the conventional thermograms.

The thermobarometric analyser was used in its commercial version (Metabolemeter from MTM Leader). This apparatus measures the variation of pressure of a sample subject to a temperature change. The sample is confined in an hermetically closed constant volume cell equipped with a pressure sensor. Thus any temperature induced volume change of the sample manifests itself as a pressure change. The pressure and temperature are simultaneously recorded to yield $P = f(T)$ curves, the thermobarograms. The measuring cell shown schematically in Fig. 1 comprises a low expansion metallic block in which a small cavity (20 mm^3) is drilled. A piezo-resistive pressure transducer operating up to 1200 bar is sealed on the bottom of this cavity. A thermocoax-type heating element coiled around the cavity ensures temperature control by means of a platinum resistance thermometer. The cell is closed by a clamp equipped with a screw device. The cell itself is located in a stainless steel block under a glass bell-type cover acting as thermal insulation. Flat soft metal (tin) gaskets are used to seal the cell cavity. We have adapted a cooling and air-pulsed system to control the temperature of the stainless steel block down to −20°C. Otherwise in normal conditions the instrument can be operated up to 250°C. The sample is placed in the cavity, which is then hermetically closed by a metallic cylinder, tightening the tin seal. In a typical experiment, once the sample has been sealed in the cell, the thermal regulation system is operated by a computer which simultaneously collects the P and T data. A second computer is used for programming and data storage operations. As a matter of fact this analyser works in an isochoric mode in the sense than it detects inside a constant volume cell, containing the sample, the pressure changes which result from programmed temperature scanning.

P–T *phase diagrams*

Several experiments (i.e. $P = f(T)$ thermobarograms) were used to obtain a complete P–T phase diagram. Each experiment was performed with an initial given free volume above the sample situated in the measuring cell. As shown in Fig. 1, this free volume corresponds to the difference between the total volume of the cavity and the actual volume occupied by the sample. This free volume is adjusted either by varying the volume of the sample or by tightening the tin gasket. The tightening is more or less controlled by means of the screw-clamp using a dynamometric wrench. However, the total volume of the cavity remains constant.

Thermobarograms of different types were obtained depending on the importance of the free volume, as shown in Fig. 2. The superimposition of the different thermobarograms on a P–T coordinate system allows one to

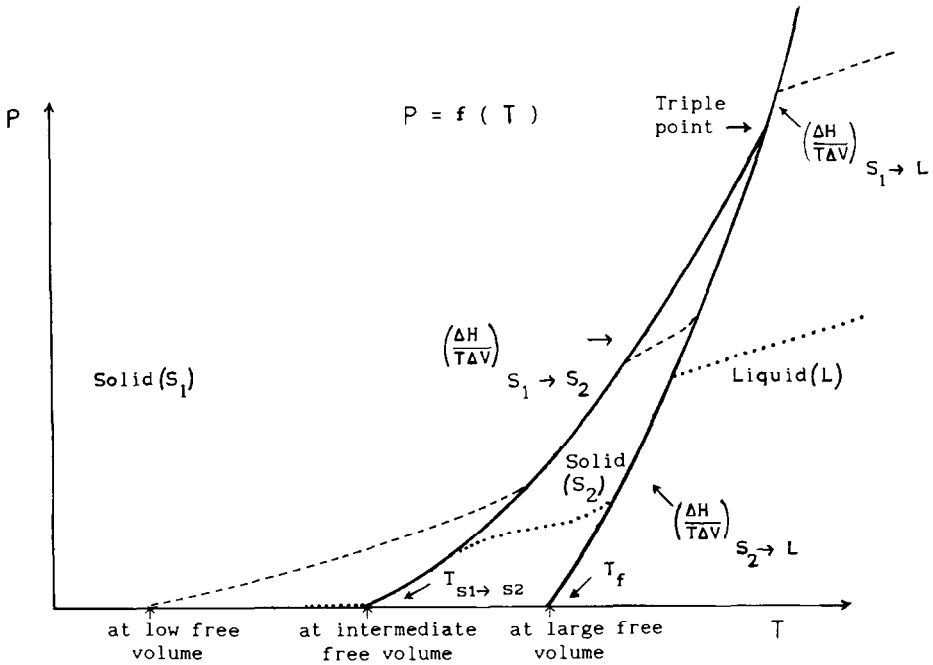

Fig. 2. Reconstitution of schematic $P = f(T)$ thermobarograms showing the influence of the free volume, and typical boundary lines in the case of a solid–solid ($S_1 \rightarrow S_2$) transition and of a solid–liquid ($S_2 \rightarrow L$) fusion.

determine the boundaries between phases in the complete phase P–T diagram.

In fact, it is necessary to distinguish along a $P = f(T)$ curve the part corresponding to a simple monophasic variation from the part associated with a diphasic transition. The thermodynamic equations related to each domain are as follows.

In the monophasic region (for the phases ph)

$$\left(\frac{dP}{dT}\right)^{ph} = \frac{\alpha_P(T)}{\chi_T(P)}$$

where α_P and χ_T characteristic of the single phase are respectively the isobaric expansibility $\alpha_P = 1/V\ (\partial V/\partial T)_P$ and the isothermal compressibility $\chi_T = -1/V\ (\partial V/\partial P)_T$.

In the diphasic region (for the transitions tr) the Clapeyron relation holds

$$\left(\frac{dP}{dT}\right)^{tr} = \frac{\Delta H}{T\,\Delta V}$$

where ΔH and ΔV are respectively the enthalpy and volume differences related to the identified phase transition.

Selected typical curves corresponding to different inital free volumes are shown together in Fig. 2; they yield the P–T phase diagram of a component exhibiting a solid–solid transition preceding a solid–liquid phase change.

RESULTS AND DISCUSSION

Results

In order to show that the two techniques used in this work are complementary, and also to illustrate their consistency, the thermograms obtained by differential scanning calorimetry and the thermobarograms and/or pressure–temperature phase diagrams obtained by thermobarometric analysis have been reported together on Figs. 3–6. In these figures the thermogram (lower part) and the P–T phase diagrams (upper part) have been represented on the same temperature scale, so permitting a direct comparison of the results at atmospheric pressure, i.e. at a pressure corresponding to the common zero baseline on each figure. The characteristic tempera-

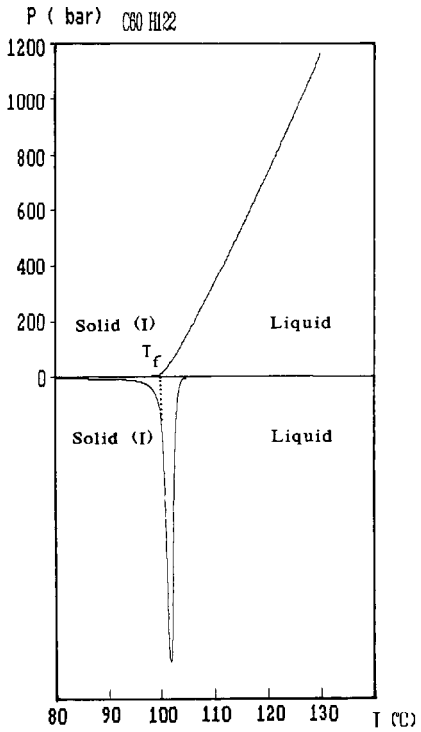

Fig. 3. Thermobarogram and thermogram of hexacontane ($C_{60}H_{122}$) showing the single transition between the orthorhombic phase I [2] and the liquid phase.

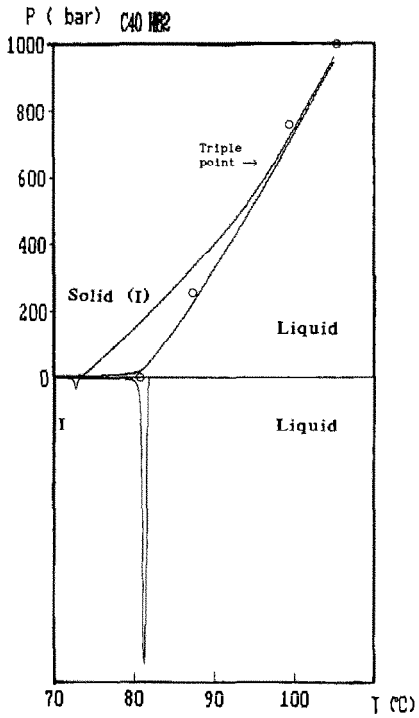

Fig. 4. $P-T$ phase diagram and thermogram of tetracontane ($C_{40}H_{82}$) showing a structural change in the solid phase from the orthorhombic phase I [2] as well as the fusion. Open circles denote characteristic temperatures from ref. 5.

tures given by the thermobarograms are obtained by extrapolation to zero of the phase transition boundary lines; the characteristic temperatures given by the thermograms are obtained by the conventional extrapolation method. Temperatures of fusion obtained with the two techniques agree within ± 1.5°C, and in most cases the difference between literature data and our present results is less than 2°C. In some cases, we have also reported for comparison the characteristic temperatures obtained by various authors using differential thermal analysis under pressure (see Figs. 4–6). A summary of the characteristic temperatures obtained and other pertinent properties extracted from the present experimental analysis are given in Table 2. For the four paraffins investigated the following observations can be made.

Hexacontane ($C_{60}H_{122}$)

The thermogram in Fig. 3 presents a single peak associated with the fusion; the thermobarogram shows a single solid–liquid transition boundary line in the $P-T$ diagram. In this particular case, when the cell is filled keeping an "intermediate free volume" (see Fig. 2), this thermobarogram

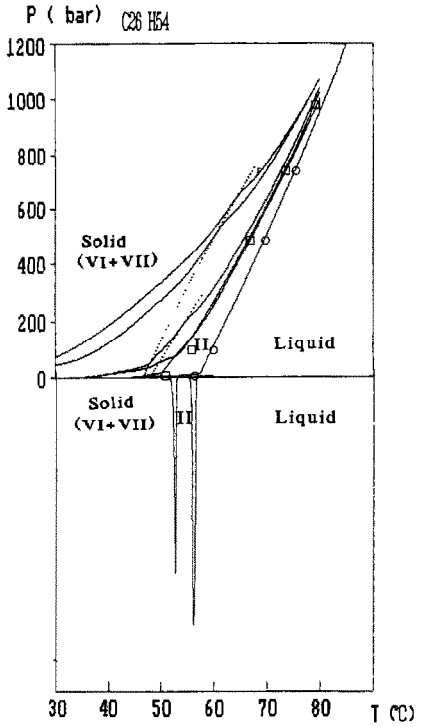

Fig. 5. $P-T$ phase diagram and thermogram of hexacosane ($C_{26}H_{54}$) showing transition in the solid phase where the monoclinic phase VI [6] and the triclinic phase VII [6] are present as well as the hexagonal phase II [6]. The equilibrium line at low temperatures in the $P-T$ diagram would correspond with the VII → VI phase change. The main peak in the thermogram corresponds to the fusion. □ and ○ denote characteristic temperatures from ref. 5.

corresponds directly to the $P-T$ phase diagram. The agreement between temperatures of fusion determined at atmospheric pressure with both instruments is satisfying and the values are close to the literature data [2], as indicated in Table 1.

Tetracontane ($C_{40}H_{82}$)

At atmospheric pressure, the thermogram in Fig. 4 reveals two peaks. The temperature of fusion is at about 80°C. The other peak obtained, close to 72°C, corresponds to a low-enthalpy solid–solid transition as mentioned by Josefiak et al. [3] at 72°C. However, under high pressure, Würflinger [5] does not mention the existence of a transition before the fusion. The thermobarograms allow the detection of two first order transitions under pressure; the phase diagram is reproduced in Fig. 4 (upper part). It is worth noting on the $P-T$ phase diagram that there is a good agreement between the temperatures of fusion from the literature and our solid–liquid

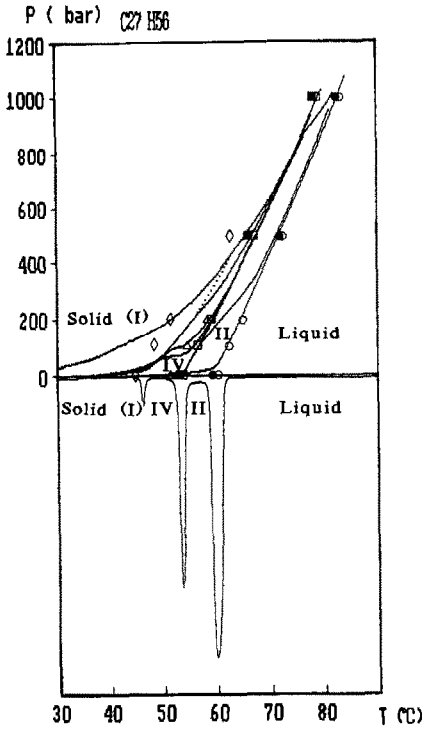

Fig. 6. $P-T$ phase diagram and thermogram of heptacosane ($C_{27}H_{56}$) showing the two transitions in the solid phase between orthorhombic phases I and IV [7] and between the orthorhombic phase and hexagonal phase II [7] respectively. ■ and ● denote characteristic temperatures from ref. 3. ◇, △, □ and ○ denote characteristic temperatures from ref. 4.

transition curve; also, the solid–solid transition boundary line appears well established. In addition a triple point, at 600 bar and 96°C, is detected, corresponding with the vanishing of the second solid phase. The solid–solid transition is slightly energetic ($\Delta H = 14$ kJ mol^{-1}, Table 2) but also exhibits a relatively low volume change ($\Delta V = 0.030$ cm^3 g^{-1}). The relatively low pressure at which the second solid phase disappears and the corresponding small energy of this solid–solid transition would explain why Würflinger [5] did not observe this transition under pressure.

Hexacosane ($C_{26}H_{54}$)

As shown in Fig. 5, the two techniques permit identification of a solid–solid transition at a temperature below that of fusion. The thermobarometric results at atmospheric pressure and under pressure are in excellent accord with the data obtained by Würflinger [5]. However, the thermobarometric curves present a more complex pattern than expected for a three phase system: at low temperature a first order transition with a

TABLE 2

Characteristic quantities and properties extracted from experimental analysis. T_f, T_{tr}: temperatures of fusion and transition respectively; ΔH_f, ΔH_{tr}: enthalpy changes for fusion and transition respectively; (α_P/χ_T): thermal pressure coefficient for solid (s) and liquid (l) phases; $(dP/dT)^f$, $(dP/dT)^{tr}$: Clapeyron slopes for fusion and transition respectively; $\Sigma \Delta H$, $\Sigma \Delta V$: total changes for enthalpy and volume respectively

	$C_{27}H_{56}$	$C_{26}H_{54}$	$C_{40}H_{82}$	$C_{60}H_{122}$
T_f (°C)	58.9	55.0	80.0	100.0
T_{tr_1} (°C)	52.2	51.2	–	–
T_{tr_2} (°C)	45.4	–	72.2	–
ΔH_f (kJ mol^{-1})	59.0	57.6	133.5	186.8
ΔH_{tr_1} (kJ mol^{-1})	26.3	32.2	–	–
ΔH_{tr_2} (kJ mol^{-1})	2.2	–	14.0	–
$\sum \Delta H$ (kJ mol^{-1})	87.5	89.8	147.5	186.8
$\left(\frac{\alpha_P}{\chi_T}\right)_1^s$ (bar °C^{-1})	2.2	2.4	8.0	12.5
$\left(\frac{\alpha_P}{\chi_T}\right)_f$ (bar °C^{-1})	8.8	9.2	8.6	7.9
$\left(\frac{dP}{dT}\right)_{tr_1}$ (bar °C^{-1})	44.9	44.3	39.2	35.6
$\left(\frac{dP}{dT}\right)_{tr_2}$ (bar °C^{-1})	37.9	33.7	–	–
$\left(\frac{dP}{dT}\right)$ (bar °C^{-1})	27.3	–	23.6	–
ΔV_f (cm^3 g^{-1})	0.103	0.106	0.169	0.165
ΔV_{tr_1} (cm^3 g^{-1})	0.055	0.079	–	–
ΔV_{tr_2} (cm^3 g^{-1})	0.004	–	0.030	–
$\sum \Delta V$ (cm^3 g^{-1})	0.162	0.185	0.199	0.165

positive pressure change of 50 bar is evident. The corresponding P–T phase diagram is given in Fig. 5 (upper part).

Heptacosane ($C_{27}H_{56}$)

As shown by the thermogram in Fig. 6, two solid–solid transitions are observed in addition to the fusion. The thermobarograms are also very sensitive to these transitions, and the comparison with data from thermal analysis under pressure shows good agreement. The P–T phase diagram is reproduced in Fig. 6 (upper part). In this case, the solid–solid transition points obtained at lower temperature by Takamizawa et al. [4] seems to deviate more than expected from the combined precisions generally accepted for the two techniques. Moreover, thermobarometric measurements seem to confirm the existence of an additional transition, approximately of first order (see dotted line on the P–T phase diagram in Fig. 6), and thus the existence of a supplementary phase stable up to 220 bar. However, this

observation is made with a precision close to the instrumental uncertainty limits, so that the above interpretation needs confirmation.

Discussion

The present study of the thermal behaviour of organic materials allows us to confirm or to establish in detail the different phase transitions. The thermophysical property data extracted from calorimetric and thermobarometric analysis are reported in Table 2. The phase coexistence boundary lines in the P–T diagram are also well defined. In particular, the triple points corresponding to the disappearance of a phase under pressure are in evidence. Clearly, the information obtained therefrom does not give insight into the nature of the solid phases detected but does indicate the combined influence of temperature and pressure on the phase diagrams. However, it is interesting to discuss the observed changes in the phase diagrams taking into consideration the information on the molecular structures given by X-ray or IR spectroscopic methods. Depending on the phases considered some aspects are of particular interest.

In the low-temperature crystalline phase

X-ray investigations by Doucet and co-workers [6,7] have shown that the phase observed at low temperature is orthorhombic as long as the carbon number of the aliphatic chain is greater than 26. In the case of hexacosane (C_{26}) its low temperature phase seems to be a mixture of monoclinic (solid VI) and triclinic (solid VII) structures. The transformation which appears at low pressure could be associated with the transformation of the triclinic into the monoclinic phase, showing a monophase domain stable with pressure and temperature for the monoclinic phase (Fig. 5). The IR investigation by Maroncelli et al. [8] indicates that at low temperature all *n*-alkanes, including long chain *n*-alkanes, have a planar conformation, with all-trans intramolecular conformers predominating. A temperature increment induces "defects" starting with the chain-ends. Then, with increasing temperature, the number of "defects" progressively increases, the crystalline structure remaining however of orthorhombic type (solid I), and this is maintained practically up to fusion in the case of hexacontane [9]. In contrast heptacosane (C_{27}) presents an important change in the number of defects when the temperature increases; this probably explains the low-energy transition observed near 45°C (see Fig. 6).

In the high-temperature crystalline phase

X-ray studies [7] of heptacosane show that when approaching fusion the crystalline structure is hexagonal (solid II). This phase, which has been studied by different techniques, is called the "rotator phase". In this phase the molecules have sufficient energy to cross over the rotation energy

barrier, allowing then a free rotation along their axes [7]. Some *cis–cis* defects ("kinks") are present in the central part of the molecule as established by IR measurements [8].

For tetracontane (C_{40}), the phase detected from our thermobarometric study (from 72 up to 80°C, at atmospheric pressure) would correspond to this "rotator phase", but the value of $(dP/dT)^{tr}$ associated with the solid–solid transition appears abnormally low compared with that for the other alkanes. Further investigations should clarify this particular point.

In the case of hexacontane (C_{60}) either thermobarograms or thermograms indicate the existence of a "rotator phase" domain. This is most likely related to the close proximity of the boundaries between orthorhombic–hexagonal and hexagonal–liquid coexistence lines. As concerns the rotative phase (solid II), it appears from the P–T phase diagram that (i) the stability domains decrease with pressure, showing the existence of possible triple points; (ii) the stability domains decrease when the chain length of the molecule increases.

CONCLUSIONS

Differential thermal analysis and thermobarometric analysis deliver the characteristic temperatures associated with the various transitions occuring in pure component phase diagrams. At atmospheric pressure, as well as at much higher pressures (above 1000 bar), the present results are in fair agreement with literature data.

The thermobarometric analysis appears even more sensitive to detect either low-enthalpy transitions or small transitions occurring at temperatures close to other major structural changes, such as fusion. In this context some particular aspects of the P–T phase diagrams can be qualitatively discussed in terms of the crystalline structures evidenced by spectroscopy.

REFERENCES

1 J.M. Buisine, B. Soulestin and J. Billard, Mol. Cryst. Liq. Cryst., 97 (1983) 398.
2 P.J. Flory and A. Vrij, J. Am. Chem. Soc., 85 (1963) 3548.
3 C. Josefiak, A. Würflinger and G.M. Schneider, Colloid Polym. Sci., 255 (1977) 170.
4 K. Takamizawa, Y. Nagao, D. Irii and Y. Urabe, Thermochim. Acta, 88 (1985) 205.
5 A. Würflinger, Faraday Discuss., Chem. Soc. 69 (1980) 145.
6 I. Denicolo, J. Doucet and A.F. Craievich, J. Chem. Phys., 78 (1983) 1465.
7 J. Doucet, I. Denicolo, A.F. Craievich and C. Germain, J. Chem. Phys., 80 (1984) 1647.
8 M. Maroncelli, S.P. Qi, H.L. Strauss and R.G. Snyder, J. Am. Chem. Soc., 104 (1982) 6237.
9 Y. Kim, H.L. Strauss and R.G. Snyder, J. Phys. Chem., 93 (1989) 7520.